Earth and Planetary Science Letters 299 (2010) 436–446

Contents lists available at ScienceDirect

Earth and Planetary Science Letters

journal homepage: www.elsevier.com/locate/epsl

# Paleomonsoon route reconstruction along a W–E transect in the Chinese Loess Plateau using the anisotropy of magnetic susceptibility: Summer monsoon model

Rui Zhang [a,b,*], Vadim A. Kravchinsky [a], Rixiang Zhu [b], Leping Yue [c,d]

[a] Department of Physics, University of Alberta, Edmonton, Alberta, Canada T6G 2G7
[b] Paleomagnetism and Geochronology (SKL-LE), Institute of Geology and Geophysics, Chinese Academy of Sciences, Beijing 100029, China
[c] State Key laboratory of Continental Dynamics, Department of Geology, Northwest University, X'ian 710069, China
[d] State Key laboratory of Loess and Quaternary Geology, Institute of Earth Environment, Chinese Academy of Sciences, X'ian 710075, China

ARTICLE INFO

*Article history:*
Received 25 March 2010
Received in revised form 17 September 2010
Accepted 21 September 2010
Available online 14 October 2010

Editor: P. DeMenocal

*Keywords:*
anisotropy of magnetic susceptibility
Chinese Loess Plateau
monsoon
paleoclimate
wind direction

ABSTRACT

The anisotropy of magnetic susceptibility (AMS) was investigated in three Chinese Loess Plateau sedimentary sections along a W–E transect (400 km). The loess–paleosol sequences in our study represent the most recent 130 kyr interval. The measured AMS was compared to expected theoretically derived magnetic fabrics occurring in strong and weak current airflow conditions. The major and minor AMS ellipsoid axis orientations were used to evaluate the paleowind direction along the transect.

Previously published models assumed that cold and dry winter monsoons bringing dust from northwestern desert areas were responsible for the magnetic fabric formation of loess sequences. In our new interpretation, the stronger summer monsoons from the southeast played the major role in magnetic fabric orientation in the studied west and central parts of the Chinese Loess Plateau. Although the material was brought to the area by the winter monsoon, the AMS was generated during the rainy summer monsoon when the sedimentary particles including magnetite were rearranged, settled, and fixed.

We reconstruct the summer paleomonsoon routes for the last 130 kyr. These winds prevail from SE to NW but appear to be affected by regional topographic factors. In the western section, the corridor between the north and south Liupan Mountains disturbed the summer monsoon route, shifting it from SE to SEE.



## 1. Introduction

Half a century ago AMS measurements were proposed as a tool for the rapid quantified description of rock fabrics in a wide range of rocks (Balsley and Buddington, 1960; Graham, 1954; Hrouda, 1982; Nagata, 1961; Rees, 1965; Stacey, 1960). Anisotropy of magnetic susceptibility (AMS) measure within a specimen is a variation of magnetic susceptibility in different orientations, described by a 3D ellipsoid that has maximum, intermediate, and minimum AMS axes. The anisotropy is determined by both the preferred crystallographic and dimensional (or shape) orientation of grains in the sediment. Superposition of ferri-, para-, and diamagnetic grain properties causes the total AMS value. The anisotropy of low-field magnetic susceptibility quantitatively measures the average preferred mineral orientation and is thus a rapid and precise tool for determining the fabric of rocks and sediments. AMS is a sensitive indicator of the texture of magnetic fabric sediment on the sediment perpetrated by wind. Consequently, wind directions can be intimated by studying the AMS of sediments deposited over time.

Heller et al. (1987) were the first to measure AMS in loess and concluded that Chinese loess had a uniform magnetic fabric and sedimentation rate through time in the Luochuan section. Further, Liu et al. (1988) demonstrated that AMS parameters could be used to evaluate the water re-working of wind-blown sediments. Thistlewood and Sun (1991) investigated a loess cross-section near X'ian in the southeast part of the Chinese Loess Plateau. Their study demonstrated that in both loess and paleosol samples the minimum axes of the AMS ellipsoids were clustered vertically and the maximum axes were gathered along the WNW–ESE direction.

Tarling and Hrouda (1993) reviewed the effects of wind and water currents on the magnetic grain fabric and AMS orientation and noticed an AMS dependence on wind/water current strength and direction. Hydrodynamic experiments have shown that gravitational forces are usually dominant and give a strong oblate fabric within the bedding plane, whereas elongated particles produce a lineation parallel to the direction of transport (Rees and Wooddall, 1975; Tarling and Hrouda, 1993). Platy minerals are usually imbricated by water currents or by wind and the minimum AMS axes tilt toward the flow direction. Stronger water currents or wind increase the tilt of the grains and can rotate and roll them causing prolate grains to align perpendicular to the current flow (Grannar, 1958). Figure 1 illustrates the dependence of the AMS ellipsoid orientation on wind/water current direction.

* Corresponding author. Department of Physics, University of Alberta, Edmonton, Alberta, Canada T6G 2G7. Tel.: +1 780 4925097; fax: +1 780 4920714.
*E-mail address:* rz1@ualberta.ca (R. Zhang).

0012-821X/$ – see front matter © 2010 Elsevier B.V. All rights reserved.
doi:10.1016/j.epsl.2010.09.026

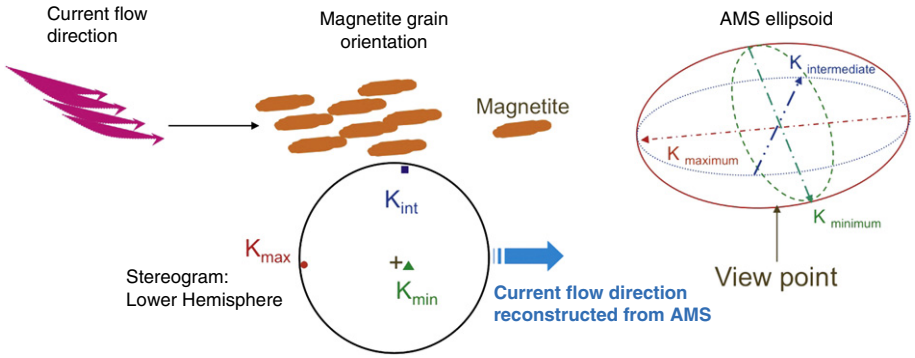


**Fig. 1.** Illustration of the mechanism responsible for orientation of the sedimentary and magnetite grains in sediment transported by strong water currents or wind. Anisotropy of magnetic susceptibility (AMS) can be illustrated with the so-called AMS ellipsoid that has a maximum susceptibility axis $K_{max}$ along the longest grain axis. The intermediate $K_{int}$ and minimum $K_{min}$ susceptibility axes are orthogonal to the maximum $K_{max}$ and define the oblateness of the AMS ellipsoid and consequently the magnetic grain. For illustrative purposes we use the lower hemisphere stereonet projection of the three-dimensional ellipsoid to define the current flow direction.

Lagroix and Banerjee (2002, 2004a,b) confirmed that the magnetic susceptibility of magnetite and maghemite in loess–paleosol sequences is three to four times greater than that of all other minerals and therefore AMS defines the magnetic lineation of the magnetite and maghemite grains. They also found that AMS measured in the central Alaska loess mirrors the overall mean paleowind directions for the same time intervals. Minor variance in the AMS orientation for different locations could denote local wind deviations.

Zhu et al. (2004) demonstrated that three magnetic minerals – primary magnetite, maghemite, and hematite – are the major carriers of the MS signal in the Chinese loess. Magnetic lineation derived from the AMS ellipsoid gathers along NE–SW and NW–SE directions during glacial and interglacial intervals in the area southeast of the Liupan Mountains. Zhu et al. (2004) reported that wind directions correspond to dust carried by the NE winter monsoon and moisture transported by the SE summer monsoon. Such NE direction is different from the commonly recognized winter monsoon course from the NW and caused by the local deviation due to Liupan Mountains. The authors noted that it is still not quite clear which of these two monsoons played a more important role in the imbrication of the magnetic grains. To further examine the role of the winter and summer monsoons in the AMS signal acquisition and to reconstruct the paleomonsoon routes, we investigated 1204 samples from three sections along an east-west transect in the Chinese Loess Plateau. The samples span the last 130 kyrs.

## 2. Sampling and methods

We sampled three sections (Baicaoyuan (36.28°N, 105.21°E), Xifeng (35.76°N, 107.7°E), and Yichuan (36.1°N, 110.14°E)) located in the western and central parts of the Chinese Loess Plateau (Fig. 2).

The dry winter monsoon brings dust from the northwest to the study area. The moist summer monsoon approaches from the southwest and brings rain. The Liupan Mountains are a natural barrier to the summer monsoon and stop some of the moisture from penetrating further west into the Baicaoyuan area. The mountain ridges protect the area from the direct influence of the summer monsoon and force the wind to change its route. These phenomena are reflected in a lower several year mean temperature (8.5 °C) and several year mean precipitation (350 mm) in Baicaoyuan compared to Xifeng (9.7 °C, 550 mm) and Yichuan (9.9 °C, 577 mm) (Banerjee et al., 1993). The study areas correspond to the semi-humid (Xifeng and Yichuan) and semi-arid (Baicaoyuan) climate.

Continuity of the eolian sedimentary sequences is highly dependent on the topography. To obtain a higher resolution AMS record we chose the most continuous and thick sections on the plateau. After removing a half-meter thick coverage along a well-exposed gully wall, we collected large blocks unaffected by weathering. The hand-cut blocks of ~10 cm width and ~20–30 cm height were orientated in-situ using a magnetic compass. Geomagnetic azimuth corrections were applied to every sample. Three smaller size cubic samples (8 $cm^3$) were cut from the same depth in the laboratory at every 2.5 cm depth interval.

The magnetic mineral content in the Baicaoyuan section and the paleomagnetism of the Xifeng and Yichuan sections have been recently discussed in Deng (2008) and Zhu et al. (2007). Magnetite is the dominant magnetic mineral in both loess and paleosol (Supplementary Material Fig. 1). The AMS, however, has never been studied at these sites. We obtained 186 samples at 10 cm intervals in the Baicaoyuan section and 523 and 496 samples from the Xifeng and Yichuan sections, respectively, at 2.5 cm intervals. The top of the Baicaoyuan section is denuded in most places and was sampled in ~30 km away from the main section. The sampled stratigraphic intervals comprised the Holocene soil ($S_0$, in our sections). The $S_0$ layer was heavily cultivated in all of our study areas and therefore the original AMS had been destroyed. Porter and An (1995) and Zhu et al. (2004) demonstrated that the Malan loess ($L_1$) corresponds to marine isotope stage (MIS) 2–4 and the interglacial soil ($S_1$) corresponds to MIS 5. Thicknesses of the sections sampled from Baicaoyuan, Xifeng, and Yichuan sections were 19, 16, and 14 m, respectively.

The mass-specific low-field magnetic susceptibility (MS) and the AMS of each sample was measured using a KLY-3 S Kappabridge (Agico Ltd., Brno) with an automated sample handling system. Each sample was rotated through three orthogonal planes. The susceptibility ellipsoid was calculated by the least-squares method; the anisotropy parameters of lineation (L), foliation (F), degree of anisotropy (P), and shape factor (T) (Jelinek, 1981) were obtained with Anisoft software using the statistical method of Constable and Tauxe (1990).

## 3. Results

In order to construct an age model, we correlated our MS record with the oxygen isotope reference curve from Bassinot et al. (1994) and with the reference Luochuan MS profile from Porter and An (1995) (Fig. 3). The Luochuan section is situated between two of our sampled sections (Xifeng and Yichuan) and is dated throughout by the thermoluminescence method (TL). To build our first order age model we correlated the MS profiles between sections and with the oxygen isotope curve from Bassinot et al. (1994). Evans and Heller (2003) discussed the necessity and success of this approach. In

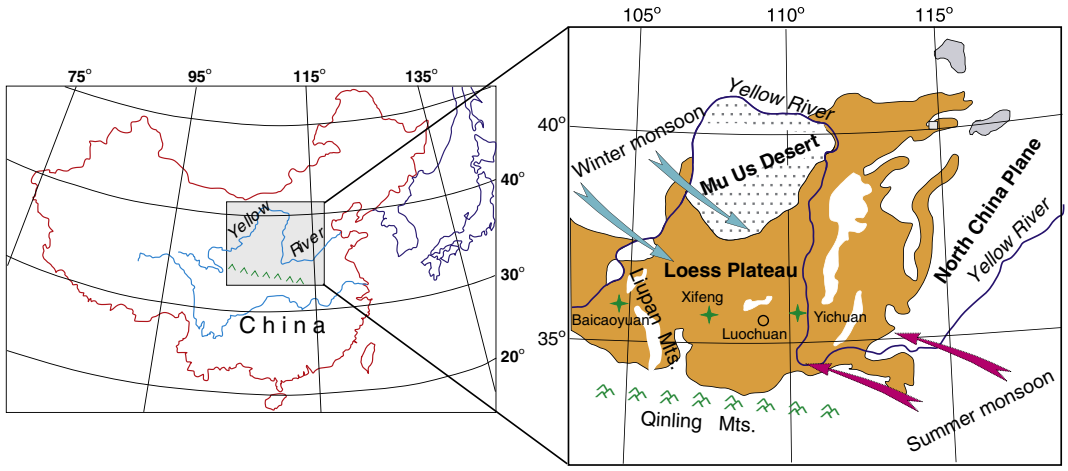


**Fig. 2.** Schematic map of the Chinese Loess Plateau showing the sampling localities discussed in the text. Dominant winter and summer monsoon directions of the present day are shown after An (2000), An et al. (2001), Porter (2001).

particular, they demonstrated that paleosols always correspond to the higher MS signals in Chinese loess/paleosol sequences due to higher concentrations of magnetite and maghemite. Our MS values for the modern soil $S_0$ and the latest paleosol $S_1$ intervals are always higher than for the loess intervals. Deng et al. (2004) showed that paramagnetic magnetic susceptibility is typically 5–8% of total MS signal in loess, and 2–4% in paleosol. Xie et al. (2009) estimation of paramagnetic effect on total MS is similar. They also concluded that the eolian contribution ~50% in the total MS signal in Chinese loess and ~30% in paleosol. It confirms that major portion of the MS signal

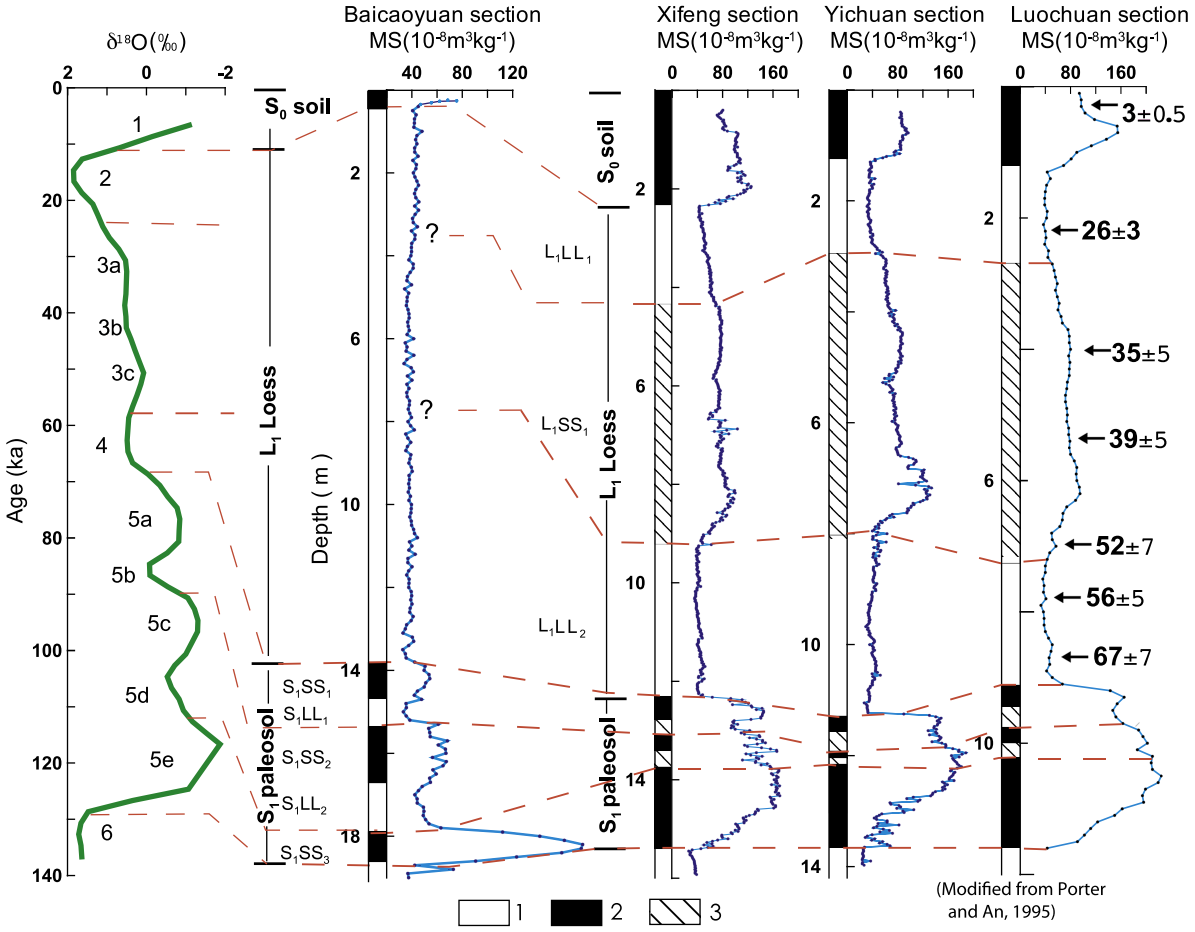


**Fig. 3.** Correlation between a marine oxygen isotope $\delta O^{18}$ reference curve (numbers signify stages), the loess/paleosol stratigraphy, and the low-field magnetic susceptibility in the studied sections. The Luochuan section parameters and TL ages are from Porter and An (1995); the marine oxygen isotope reference curve is from Bassinot et al. (1994). 1 — loess intervals, 2 — paleosol intervals, 3 — underdeveloped paleosol.

in loess and large portion of the signal in paleosol are determined by the ferromagnetic minerals transported by the wind.

In order to adjust our first order age model based on correlation with the oxygen isotope curve (Fig. 3) we applied a correlation to the reference Luochuan section which has TL dates published by Porter and An (1995). The final results of this correlation and our age model are presented in Supplementary Material Table 1. The rapid changes in susceptibility values at the $L_1/S_0$, $S_1/L_1$, and $L_2/S_1$ stratigraphic boundaries correlate well with the MIS 2/1 (12.05 kyr), MIS 5/4 (73.91 kyr), and MIS 6/5 (128 kyr) boundaries. The loess horizon $L_1$ has higher MS values in the middle part of the profile in Xifeng, Yichuan, and Luochuan sections because of the magnetic signal enhancement caused by the paleosol horizon $L_1SS_1$ (Fig. 3). The horizon corresponds to MIS 3. Two warming intervals in MIS 3 (around 29 and 53 ka) are prominent in all cross-sections except the Baicaoyuan. We suppose that dry climate conditions existed in the Baicaoyuan area during MIS 3. Such dry conditions could have been caused by a relatively high rate of Liupan Mountain growth as a result of the continuous penetration of India into the Eurasian continent. The mountains would block the summer monsoon moisture from infiltrating further west into the continent. Xifeng, Yichuan, and Luochuan had more moisture and the $L_1SS_1$ horizon is well preserved in these sections. Although the precise time and amplitude of Liupan Mountain growth is difficult to determine, the 2000 m uplift of the Himalayan mountains and Tibet during the Pleistocene epoch is well known (Li, 2006; Rieser et al., 2009).

The relatively warmer and cooler stages of MIS 5 are well represented in all four sections. For the Baicaoyuan section, however, three subdivided paleosols ($S_1SS_1$, $S_1SS_2$, $S_1SS_3$) and two intrabedded loess units ($S_1LL_1$, $S_1LL_2$) are better pronounced inside the MIS 5 pedocomplex ($S_1$). The Liupan Mountains perhaps had lower elevation than today and did not block all the summer monsoon moisture during MIS 5 allowing a generally more humid climate and soil formation than during MIS 3 and today.

The low field AMS is generally described in the sample by an oriented ellipsoid with maximum ($K_{max}$), intermediate ($K_{int}$), and minimum ($K_{min}$) axes of magnetic susceptibility. Following the technique suggested by Lagroix and Banerjee (2004b) and applied in Zhu et al. (2004), we used epsilon $\varepsilon_{12}$ which represents the half-angle uncertainty of $K_{max}$ in the plane joining $K_{max}$ and $K_{int}$ and $\varepsilon_{23}$ which is the half-angle uncertainty of $K_{int}$ in the plane joining $K_{int}$ and $K_{min}$. In these notations, 1, 2 and 3 are assigned to $K_{max}$, $K_{int}$ and $K_{min}$, respectively. An inverse relationship between $\varepsilon_{12}$ ($\varepsilon_{23}$) and the magnetic lineation parameter L (magnetic foliation parameter F) was observed in all sections (Fig. 4a and c demonstrates that L (F) decreases as $\varepsilon_{12}$ ($\varepsilon_{23}$) increases) due primarily to the increasing importance of random measurement errors for $K_{max}$ ($K_{min}$) in the lineation (foliation) plane with weak lineations (foliations). Independence between $\varepsilon_{12}$ and foliation (Fig. 4b) reinforces the fact that the lineation and foliation sub fabric could be defined by separate mineral orientation distributions. The majority of the samples from all three studied localities demonstrate the prevalence of oblate magnetic fabric which is typical for loess (Lagroix and Banerjee, 2004b); nevertheless the presence of prolate grains is evident (Fig. 4). The majority of the samples satisfies the statistically significant level of $\varepsilon_{12}<22.5°$ (70.1% for BCY, 86.6% for XF, and 92.3% for YC).

The $K_{min}$ directions are described by the inclination (I–$K_{min}$) and declination (D–$K_{min}$) of $K_{min}$ distributed along the vertical axis of the stereonet projection. I–$K_{min}$ is larger than 70° in 87.7%, 78.0%, and 62.2% of our samples from Baicaoyuan, Xifeng, and Yichuan, respectively, corresponding (usually) to an undisturbed (less reworked) loess with an observed oblate fabric.

Figure 5 illustrates the principal orientations of the minimum and maximum susceptibility axes ($K_{min}$ and $K_{max}$). The majority of $K_{max}$ are distributed along the edge of the stereonets in the Baicaoyuan section. The declinations and inclinations of $K_{max}$ and $K_{min}$ in the stereonet projection are illustrated by a single point for each sample in Figure 5a. Figure 5d demonstrates selected samples for which $\varepsilon_{12}<22.5°$ and $I-K_{min}>70°$. Samples were selected using the technique suggested by Lagroix and Banerjee (2004b) and Zhu et al. (2004) in order to isolate the most significant $K_{max}$ declination. All $D-K_{max}$ with $\varepsilon_{12}>22.5°$ were rejected to eliminate noisy directions. Lagroix and Banerjee (2004b) discuss this approach and suggest such filter because $\varepsilon_{12}=22.5°$ yields a confidence ratio of 1.0 for maximum and intermediate susceptibility axes in the foliation plane. The rejection of inclinations $I-K_{min}$ lower than 70° provides that only undisturbed sediments are considered. Alternatively we applied contour lines and rose diagrams to illustrate the distribution of $K_{max}$. Figure 5b and c illustrate the distributions of $K_{max}$ and $K_{min}$ directions for all samples and Figure 5e and f visualize the same for selected samples with $\varepsilon_{12}<22.5°$ and $I-K_{min}>70°$. To construct the contour lines of the stereonet projections we followed the computing method described by Robin and Jowett (1986) that calculates the point distribution densities and their significance over the lower hemisphere. The method allows us to observe higher concentrations in the sample and to appreciate the significant discrepancy from a uniform distribution.

Rose diagrams for $D-K_{max}$ are a favorite method of depicting orientations because of their ease of comprehension. To construct the rose diagrams in Figure 5b and e, we split the stereonet into an equal number of 10° segments; each segment on the stereonet represents a number of samples and the direction of the $D-K_{max}$. The longest segments of the rose diagrams and the peak orientation (maximum density of the contour lines) signify the larger number of samples in the specific direction. Without considering the inclination, the rose diagram magnifies only variations in $K_{max}$ declinations. $K_{max}$ has the majority of samples oriented along the NEE direction in the loess horizon $L_1$ (maximum is at $D-K_{max}=95°$ from the contour distribution, and it is 90–100° from the rose diagram analysis of Fig. 5b). The maximum axis susceptibility has two major values in the paleosol horizon $S_1$ at $D-K_{max}=105°$ and at $D-K_{max}=69°$. The contour lines in Figure 5c and f represent the distribution of $K_{min}$ axes on the stereonet projection. The majority of the minimum susceptibility directions are located near the vertical plane with notable imbrications toward the NW (Fig. 5c and f). The peak orientation of the contour lines and rose diagram for loess and paleosol are fairly close to each other ($D-K_{min}=323°$, $I-K_{min}=85°$ for $L_1$ and $D-K_{min}=324°$, $I-K_{min}=85°$ for $S_1$) and to the major route direction of the present day summer monsoon (An, 2000; An et al., 2001; Porter, 2001).

Combined analysis of all units in the Xifeng section indicates that the $K_{max}$ directions are distributed along a girdle primarily toward the SE (Fig. 6b and e). The peak orientation of $K_{max}$ indicated by the maximum density of the contour lines or the longest section of the rose diagram is $D-K_{max}=130°$ for $L_1$ and $D-K_{max}=125°$ for $S_1$ in samples depicted in Figure 6b and e. The preferred orientation of the minimum AMS axis is tilted to the NW (Fig. 6c and f). The peak orientation of the contour lines for loess and paleosol are close to each other ($D-K_{min}=328°$, $I-K_{min}=86°$ for $L_1$ and $D-K_{min}=327°$, $I-K_{min}=80°$ for $S_1$), similar to other sections, and correspond to the present day summer monsoon path.

Figure 7 illustrates the AMS inclinations and declinations for the Yichuan section. The major SE direction of $L_1$ and $S_1$ units in the Yichuan sections are well illustrated by the contour lines and the rose diagram in Figure 7b and e. The orientation of the AMS ellipsoid indicated by the peak orientation or the longest section of the rose diagram has $D-K_{max}=131°$ for $L_1$ and $D-K_{max}=151°$ for $S_1$ for samples with $\varepsilon_{12}<22.5°$ and $I-K_{min}>70°$. The peak orientation of $K_{min}$ or the longest section of the rose diagram tilted to the NW has $D-K_{min}=323°$, $I-K_{min}=87°$ for $L_1$ and $D-K_{min}=297°$, $I-K_{min}=86°$ for $S_1$.

Additionally we performed analysis of the AMS results of selected samples with $\varepsilon_{12}<11.25°$ and $I-K_{min}>70°$ for the studied sections (see on-line Supplementary Material Fig. 2). These results coincide

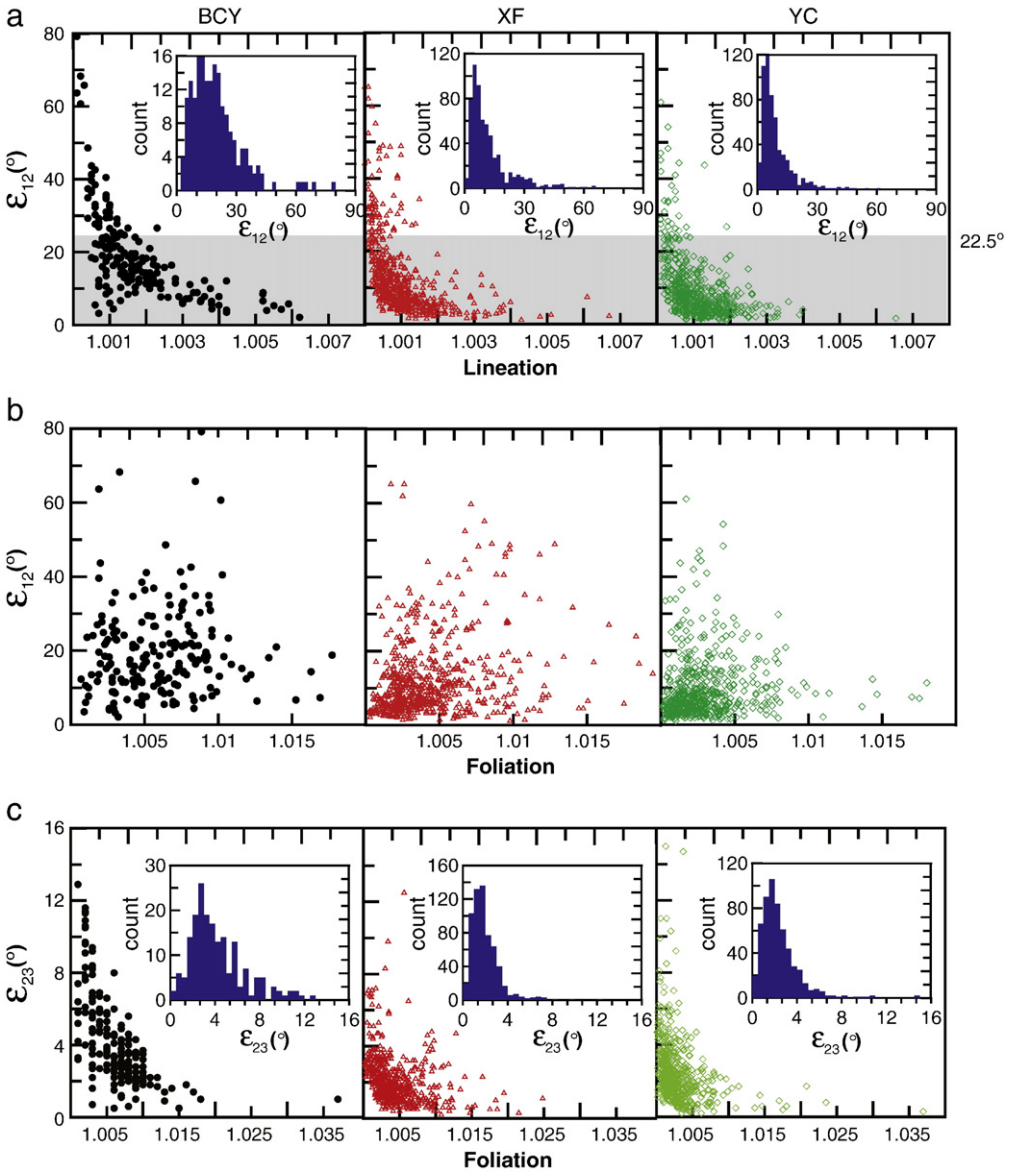


**Fig. 4.** (A) Plots of $\varepsilon_{12}$ (the 95% confidence ellipse of $K_{max}$ in the plane joining $K_{max}$ and $K_{int}$) against lineation. The plots demonstrate inverse relationship between $\varepsilon_{12}$ and lineation. (B) Plots of $\varepsilon_{12}$ against foliation. The plots demonstrate independence between $\varepsilon_{12}$ and foliation. (C) Plots of $\varepsilon_{23}$ (the 95% confidence ellipse of $K_{min}$ in the plane joining $K_{min}$ and $K_{int}$) against foliation. BCY — Baicaoyuan, XF — Xifeng, and YC — Yichuan sections. The inserts are the frequency distributions of $\varepsilon_{12}$ using 2° bin sizes and $\varepsilon_{23}$ using 0.5° bin sizes. They demonstrate that majority of the samples satisfies statistically significant level of $\varepsilon_{12}<22.5°$ (70.1% for BCY, 86.6% for XF, and 92.3% for YC). The significance level of $\varepsilon_{23}$ is $<11.25°$ for absolute majority of the samples.

with the findings of the preferable AMS orientation using all samples and samples with $\varepsilon_{12}<22.5°$.

## 4. Discussion

The contour lines and rose diagrams in Figures 5–7 illustrate the statistically preferred orientation of the AMS in the sections studied. The declination of the $K_{max}$ mean directions ($D-K_{max}$) is nearly horizontal and is projected on the edge of the stereonets. We calculated the peak orientations (declinations and inclinations) for $K_{max}$ and $K_{min}$ for the studied sections using contour lines (Supplementary Material Table 2). The peak orientations demonstrate that the preferred orientation of the elongated particles was in the SE direction in the Xifeng and Yichuan sections and in the SEE direction in the Baicaoyuan section. Such orientations indicate that the prevailing paleowind direction was from the SE and SEE on a local scale. Furthermore, the majority of the samples have minimum axes oriented vertically with their peak orientations tilted towards the NW (323°/86°, 325°/85°, and 307°/86° in Baicaoyuan, Xifeng, and Yichuan, respectively). Tarling and Hrouda (1993) and Zhu et al. (2004) demonstrated that the wind tends to change the sedimentary grain orientation and to tilt the longest axes of the grains as demonstrated in Figure 1. The minimum AMS axes would be imbricated to a downstream direction (NW in our cases) by small angles (<20°).

In order to explore statistical significance of our results we calculated the mean directions and corresponding error ellipsoids for the studied sections using Bootstrap statistics (Constable and Tauxe, 1990) additionally to the maxima analysis of rose diagrams and contour lines. The results are similar for Baicaoyuan section and deviate from each other only slightly for Xifeng and Yichuan sections (Supplementary Material Fig. 3, Supplementary Material Table 3). The $K_{max}$ and $K_{min}$ orientations demonstrate that the preferred wind direction was from SE and SEE. The Bootstrap statistics treats the AMS ellipsoid as a tensor with three orthogonal eigenvectors ($K_{max}$, $K_{int}$ and $K_{min}$). The Bootstrap statistics calculation clearly demonstrates that the mean $K_{min}$ orientations are statistically different from the

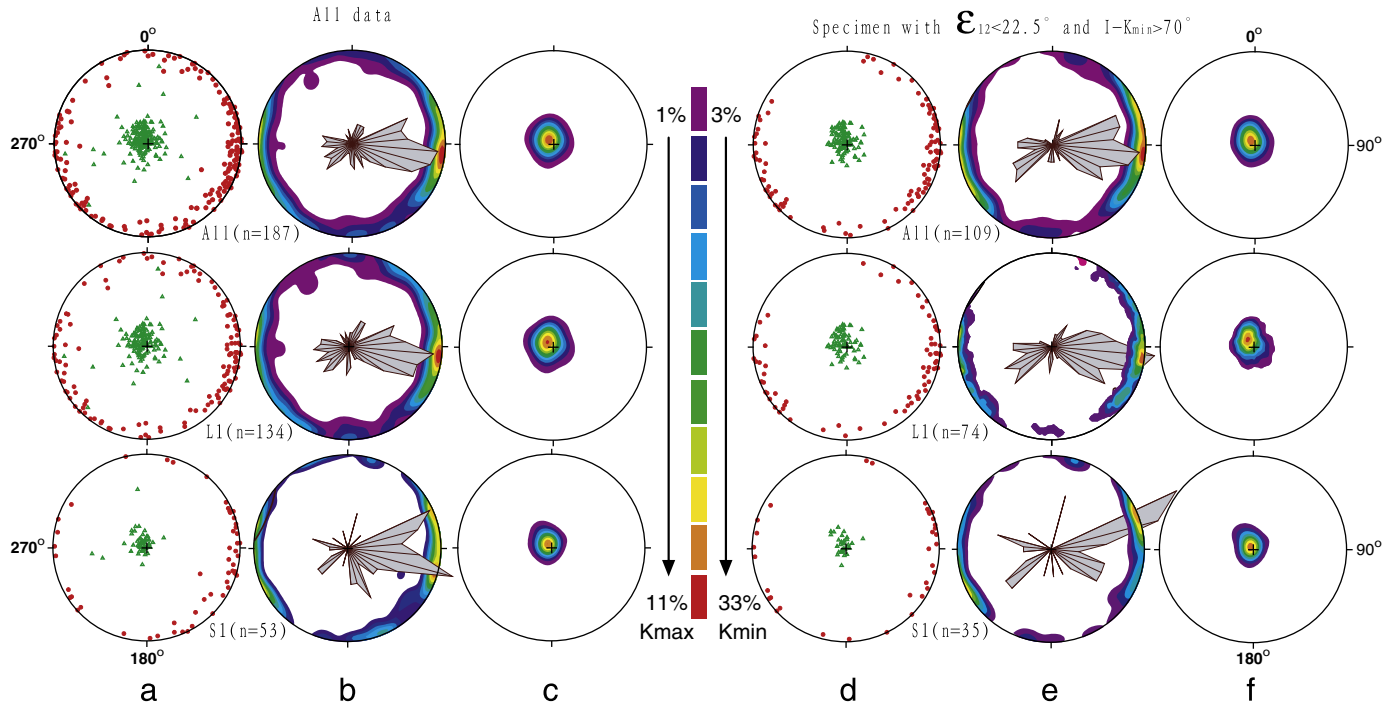


**Fig. 5.** AMS results for the Baicaoyuan section: stereographic projection of $K_{max}$ (red dots) and $K_{min}$ (green triangles) (a, d); contours and rose diagram of $K_{max}$ (b, e); contours of $K_{min}$ (c, f). Parameter n is a number of samples included to the analysis. Legend corresponds to a percentage of the samples falling in the indicated by the color contour lines for $K_{max}$ (left) and $K_{min}$ (right).

vertical axis in every studied locality and can be evaluated in terms of imbrication of the ferrimagnetic and paramagnetic particles. At the same time the tensor's average for $K_{max}$ displays the noticeable difference between peak orientation and Bootstrap mean direction. One can use either peak orientation or Bootstrap mean for the paleowind direction reconstruction. The rose diagrams illustrate that the orientation distribution of $K_{max}$ and $K_{min}$ are not perfectly aligned in the opposite directions (Supplementary Material Fig. 3), as it would be expected if only prolate particles are present. The AMS of a measured cubic specimen is the sum of each particle AMS. The crystallographic axes of the particle control AMS of a silicate particle (Lagroix and Borradaile, 2000). Magnetite and maghemite, due to

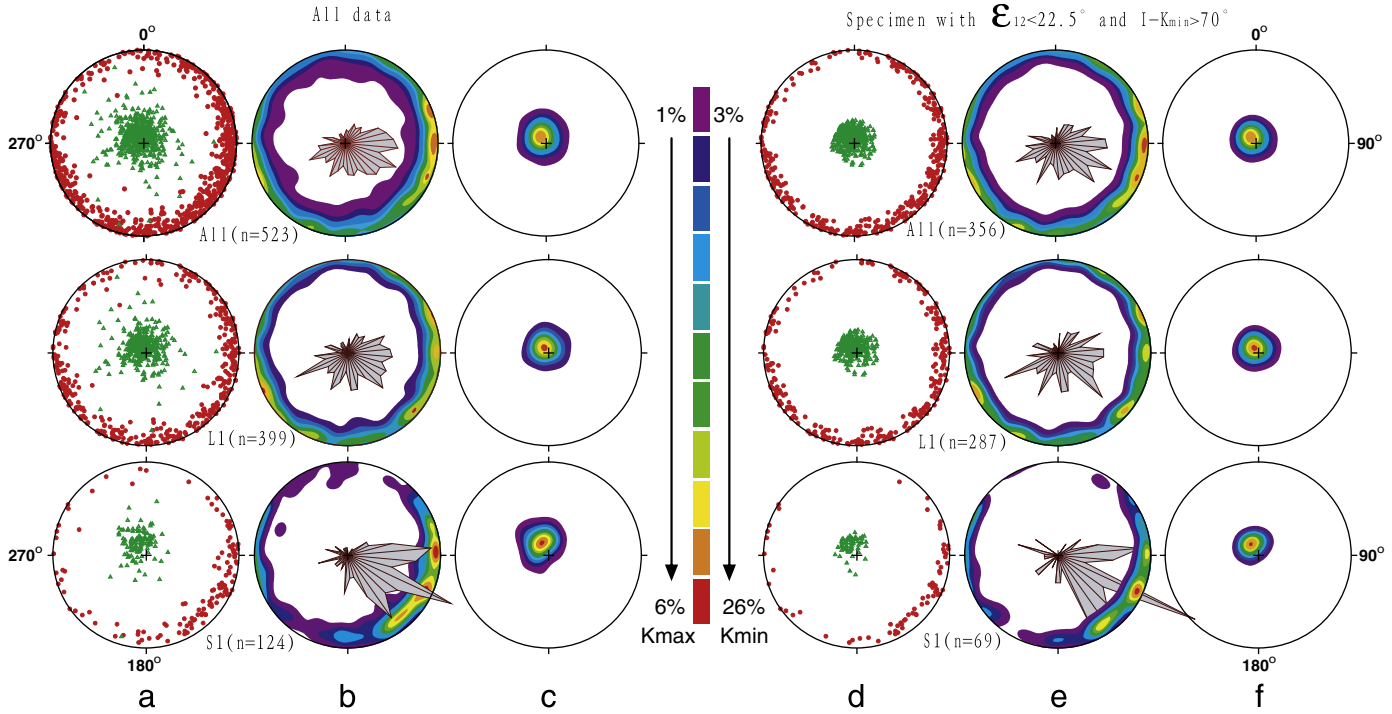


**Fig. 6.** AMS results for the Xifeng section: stereographic projection of $K_{max}$ (red dots) and $K_{min}$ (green triangles) (a, d); contours and rose diagram of $K_{max}$ (b, e); contours of $K_{min}$ (c, f). Parameter n is a number of samples included to the analysis. Legend corresponds to a percentage of the samples falling in the indicated by the color contour lines for $K_{max}$ (left) and $K_{min}$ (right).

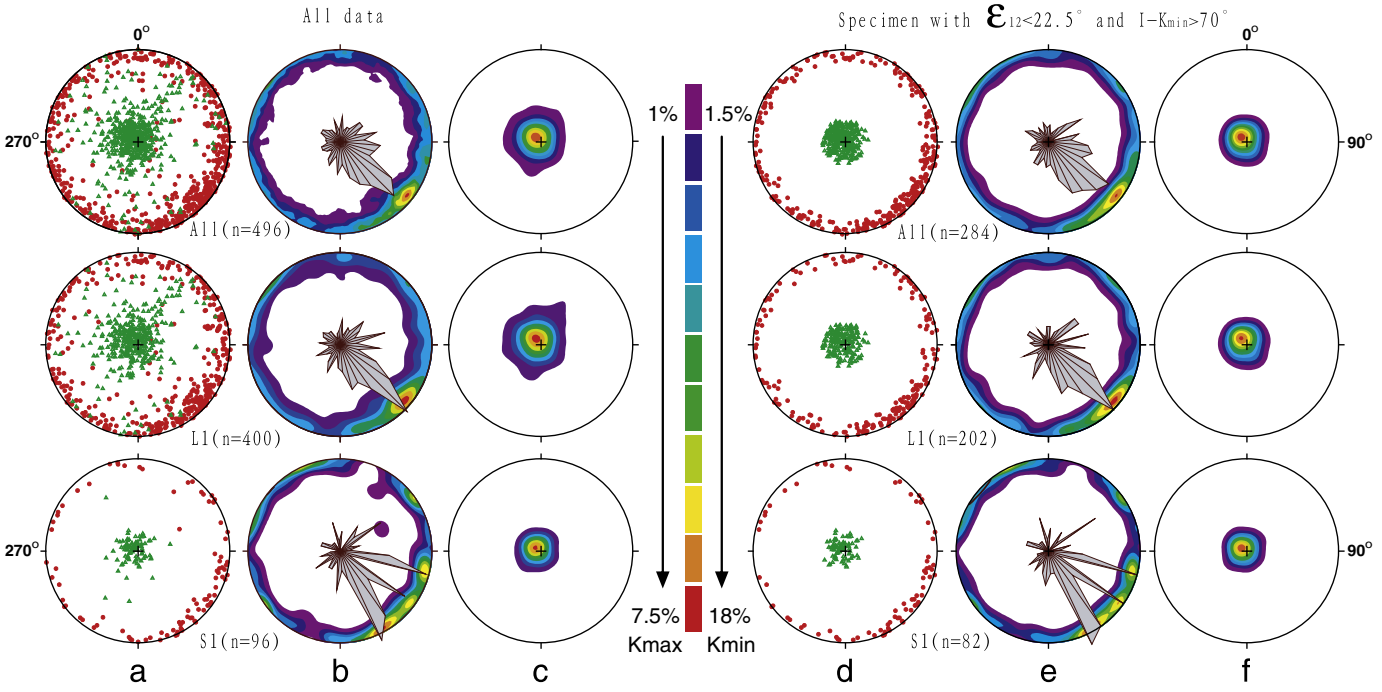


**Fig. 7.** AMS results for the Yichuan section: stereographic projection of $K_{max}$ (red dots) and $K_{min}$ (green triangles) (a, d); contours and rose diagram of $K_{max}$ (b, e); contours of $K_{min}$ (c, f). Parameter n is a number of samples included to the analysis. Legend corresponds to a percentage of the samples falling in the indicated by the color contour lines for $K_{max}$ (left) and $K_{min}$ (right).

their strong intrinsic magnetization and internal demagnetizing field, have AMS controlled by the particle shape where the maximum susceptibility axe is parallel to the grain's long dimension in multi/pseudo domain particles. In stable single domain particles the maximum susceptibility axe is perpendicular to the grain's long dimension. At the particle level, silicates generally give oblate AMS ellipsoid, while magnetites give prolate AMS ellipsoids. The orientation distribution of the magnetite particles versus the silicate particles controls the AMS at the specimen level. The peak orientation of the $K_{max}$ distribution represents the elongate magnetite grain's orientation while $K_{min}$ is always contaminated by the distribution of the oblate silicate mineral particle's short dimension. Therefore for our paleowind direction reconstruction we prefer to use the peak orientation of $K_{max}$ from the contour lines. We use $K_{min}$ only as an additional factor to determine that apparently the SE direction of the wind caused the particle's imbrications. The different statistics techniques, however, coincide generally between each other in our study and do not alter our conclusions.

Hus (2003) and Thistlewood and Sun (1991) showed that the winter monsoon that comes primarily from the northwestern central Asian desert areas carries a majority of the sedimentary particles and determines the magnetic fabrics' orientation in the loess and paleosol horizons.

Wind tunnel experiments (Wu et al., 1999) showed that eolian deposition is analogous to deposition under hydrodynamic conditions (Rees and Wooddall, 1975; Tarling and Hrouda, 1993). These experiments showed a strong correlation with deviations less than 20° from the actual current direction. In the samples investigated here we compared the $K_{max}$ and $K_{min}$ directions with the theoretically predicted depositional fabrics that would be expected under hydrodynamic flow (Tarling and Hrouda, 1993) and with laboratory results for running water experiments (Rees and Wooddall, 1975). Figure 8 illustrates the results of these studies. When deposition occurs in still water, gravitational settling is the only significant force and the majority of rod-like ferromagnetic grains are arranged with their longer axes aligned randomly within the bedding plane. This gives rise to a simple oblate fabric in the bedding plane (Fig. 8a). Under a weak water current, most elongated magnetite grains line up parallel to the direction of the current and the superposition of gravity and current forces causes most of the maximum AMS axes to tilt to the upstream direction and the minimum axes ($K_{min}$) to tilt to the downstream direction (Fig. 8b). The prolate grains are more stable when their longest axes lie perpendicular to the direction of water flow. The stronger the current, the higher the tendency of prolate particles to become oriented perpendicular to the current flow (Fig. 8c, d).

We suggest a simple explanatory model to explain our AMS results. Current theory states that relatively cold and dry winter monsoon is a major driving force of the grain orientation that yields magnetic fabric (Thistlewood and Sun, 1991). Magnetic fabric is formed by the superposition of gravity and wind forces (Fig. 9). The wind carries eolian material in the air while gravity pulls the sedimentary grains to earth. On the ground, sedimentary grains are reoriented by wind until they are covered by a new layer of eolian sediment. As layers accumulate on top, the loess becomes immobile and finally solidifies. Magnetic minerals remain ambulant until they solidify. Before burial and eventual solidification, eolian material can be transported back and forth from air to ground if the wind is strong enough. Consequently the particles could probably be rearranged again until they are fixed in the sedimentary layers. Rain and more wind are brought by the moist summer monsoon which approaches from the SE, a direction opposite to that of the winter monsoon (Fig. 2). We suggest that the summer monsoon wind in the study area (west and center of the Chinese Loess Plateau), which is stronger than the winter monsoon wind (Supplementary Material Fig. 4), is strong enough to rearrange the sedimentary particles in the study areas again. The rain often falling during the summer does not allow the wind to displace the particles far from the site and finally fixes them in the loess or soil layer. New formed magnetite particles at the top of the soil are also reoriented by the summer wind and rain. The rapidly developing summer vegetation covers the newly-formed loess/soil layer and the plant roots do not allow the next winter monsoon to re-orient the grains of the solidified layer. The main process likely occurs during one year although some later compaction of the loess could still take place and cause certain 'noise' in our measurements. The new magnetite formed by pedogenesis processes in the deeper soil

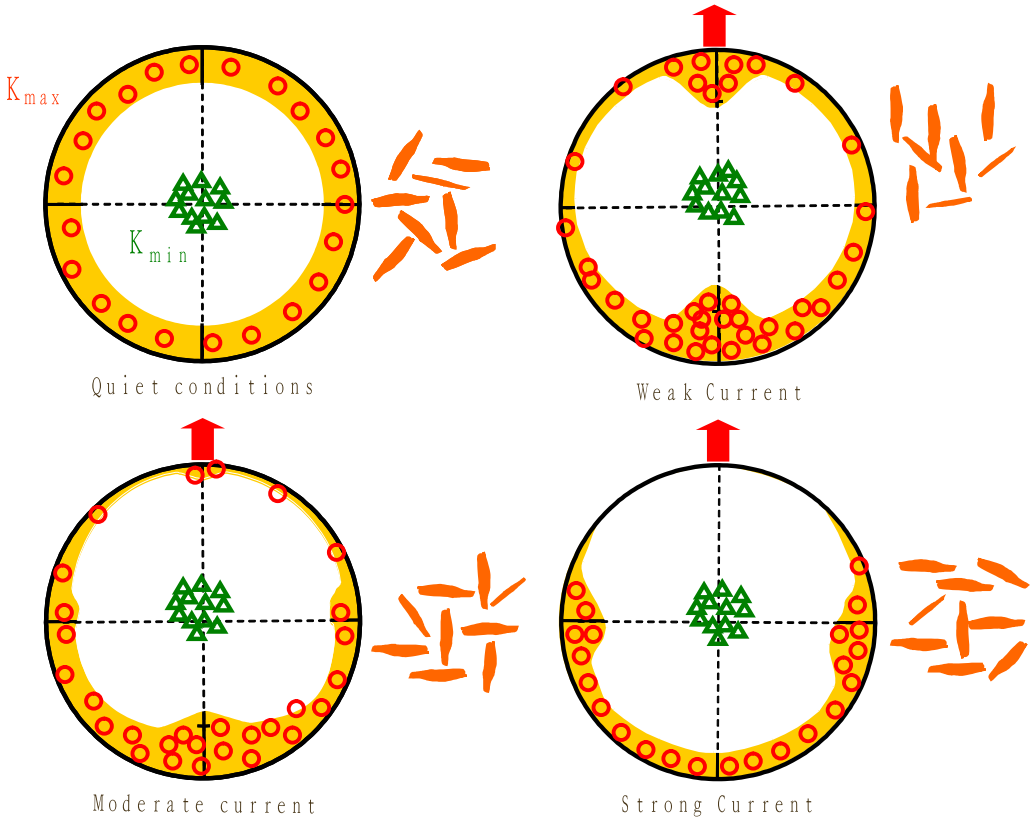


**Fig. 8.** Theoretical depositional fabric in the presence of water currents (revised from Tarling and Hrouda (1993)). The red and green areas in the diagrams represent the orientations of $K_{max}$ and $K_{min}$, respectively. The orange grains to the right of each stereonet illustrate the preferred alignment of most magnetic particles in the horizontal plane.

layers under surface additionally enhanced the total MS signal but not necessary AMS values. Our model also implies that a lock-in depth phenomenon does not affect at least studied $S_1$ and $L_1$ horizons. Such possibility was recently debated by Zhu et al. (2006) for $L_1$ loess and Liu et al. (2008b) for Brunhes/Matuyama boundary.

We consider that both $K_{max}$ and $K_{min}$ orientations could be correlated to the predominant paleowind direction during the summer monsoon in the Chinese Loess Plateau regions. The mean AMS axes directions in the loess horizon $L_1$ and paleosol horizon $S_1$ are both in the SE quarter of the stereonet and broadly correspond to the course of the summer monsoon (Fig. 9).

We compared our result with the present day regional wind directions using the on-line publically available tool from Physical Sciences Division of Earth System Research Laboratory (National Oceanic and Atmospheric Administration, U.S. Department of Commerce) (Supplementary Material Fig. 4). Surface wind directions and

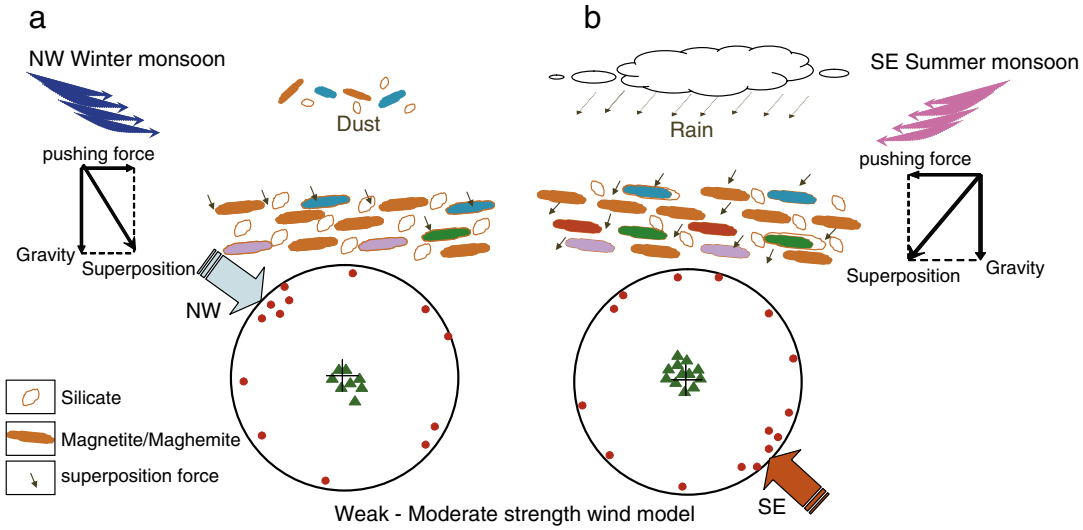


**Fig. 9.** A model of AMS that depends on the monsoon directions in the southern part of the Chinese Loess Plateau. (a) The winter monsoon brings sedimentary and magnetic particles with the dust from the NW. The AMS ellipsoid would reflect the prevailing orientation of the particles as shown in the stereonet below (lower hemisphere projection). (b) The summer monsoon brings rain and wind from the SE, reorienting and finally fixing sedimentary and magnetic grains in the uppermost seasonally formed layer of loess or soil. The AMS ellipsoid is now oriented in a direction opposite to the winter monsoon direction. Rain helps to settle the sedimentary and magnetic grains and the growing summer vegetation fixes them in-situ. Grains become immobile. The next winter monsoon covers the site with new eolian material and the process repeats.

speed for the winter months of November–March (Supplementary Material Fig. 4A) and the summer months of May–September (Supplementary Material Fig. 4B) are calculated from the 1950 to 2009 monthly long-term means. The regional winter monsoon wind in the study area is dominantly from north-west and south-south-west. The winter wind is however relatively weak (1–2 m/s) when comparing to the summer monsoon wind strength (2–3 m/s). The strong winter monsoon wind in the desertic areas north of Chinese Loess Plateau carries the dust particles to the Plateau where the particles are deposited (the winter monsoon wind over the Plateau is too weak to carry the particles further). The stronger summer monsoon wind from SW and SSW in the study area of the Plateau is continuously accompanied by the rain and moister which does not allow the loess particles to be transported away from the Plateau.

The model for Chinese Loess Plateau interglacial horizon, i.e. paleosol, formation implies that up to 70% of the particles responsible for the MS signal are crystallized in-situ and are not transported by the wind (Evans and Heller, 2003; Xie et al., 2009). Since we observe that the dominant fabric orientation in loess and paleosol is similar, the prevailing winds are able to reorient grains that are on the ground. Maher and Taylor (1988) were first to demonstrate that the peak neo-formation of fine-grained ferrimagnetics in the modern topsoil is not exactly at the surface but more commonly a few centimeters below the surface. In the specimen we cannot separate AMS of detrital and pedogenic magnetite but our data demonstrate that overall the AMS signal in $S_1$ horizons is as strong as in $L_1$ horizons (Figs. 5–7). We suggest that although the neo-formed magnetite particles contribute to the higher MS values, they are predominantly chaotically oriented in terms of preferred axis orientation and therefore the individual AMS of pedogenic particles generally cancel each other's effects. This way the detrital contribution from the particles arranged by the summer monsoon still dominates the total AMS signal.

Figure 10 depicts the spatial variations of the preferred paleowind directions along the Loess Plateau. The contour lines and rose diagrams are separated for loess $L_1$ and paleosol $S_1$ combined in every section, while actually there is no significant difference in AMS orientations between soil and loess horizons. In our model the orientations of $K_{max}$ in Yichuan (the upwind azimuth is 129°), Xifeng (128°), and Baicaoyuan (96°) are associated with the summer monsoon coming from the SE in the whole dataset. We observe a shift of ≈32° in the monsoon route for the Baicaoyuan section which is located to the west of the WE corridor between the north and south Liupan Mountains. We assume that the mountains cause the monsoon to deviate and propagate deeper into the continent in the Baicaoyuan area. Such local wind deviation does not contradict the present day regional wind course in the study area (Supplementary Material Fig. 4).

The primary SEE directions in the Baicaoyuan section are similar to the weak current model (Tarling and Hrouda, 1993) in Figure 8 because the majority of individual $K_{max}$ orientations in the sample are parallel to the direction of the summer monsoon, forming primary SEE and

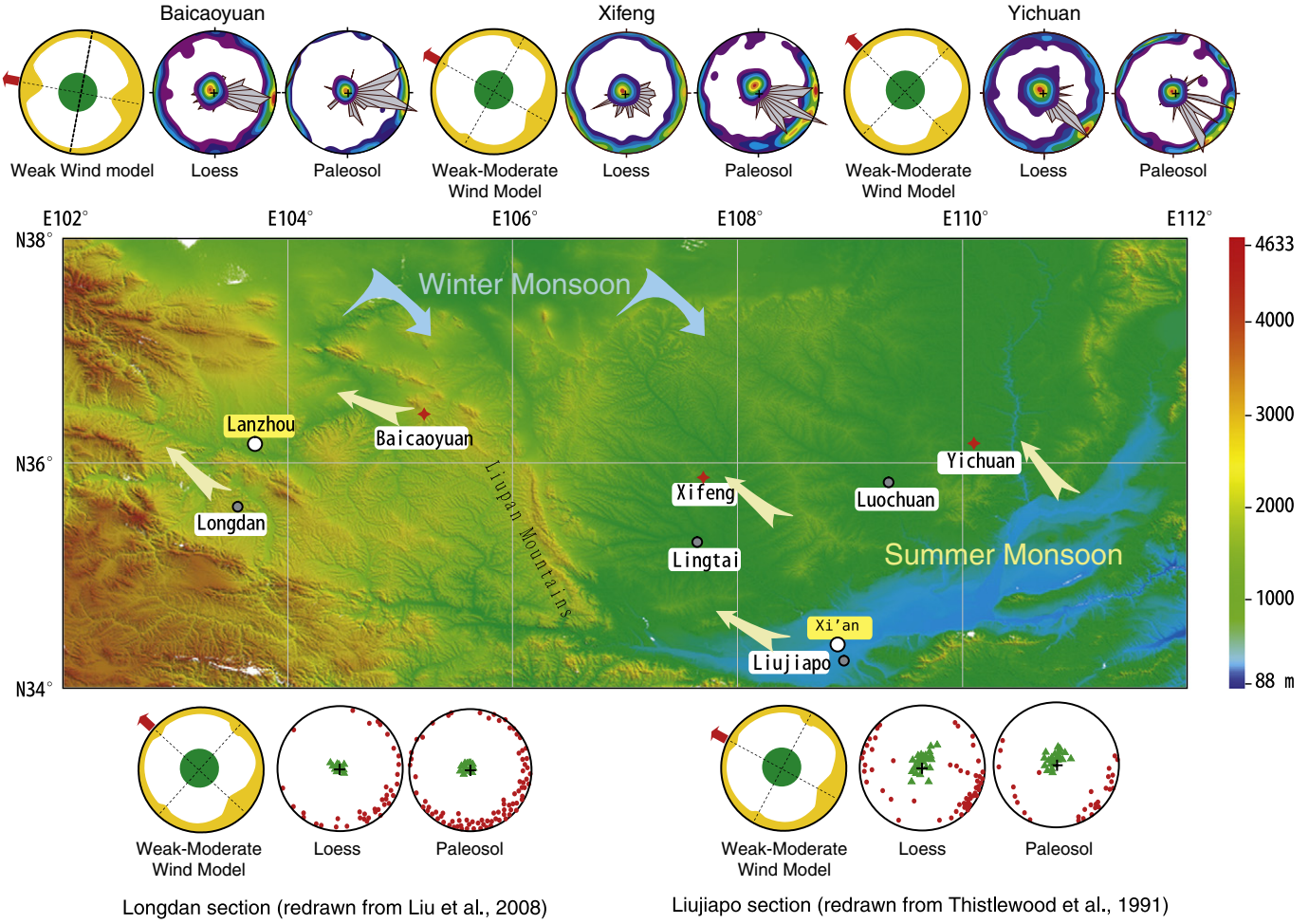


**Fig. 10.** Dominant summer monsoon routes for last 130 kyrs reconstructed from our AMS analysis along the west-central transect across the Chinese Loess Plateau. Arrows illustrate the ancient summer monsoon wind direction; the relative strength of the wind is specified by the comment near each local wind model stereographic projection. Above: lower hemisphere stereographic projections showing the contour lines and rose diagrams for $K_{max}$ for all studied samples with arrows pointing toward major summer monsoon directions in every locality. Below: lower hemisphere stereographic projection of $K_{max}$ and $K_{min}$ from two other localities. Note that original figures in Thistlewood and Sun (1991) are shown for the upper hemisphere.

secondary NWW directions. In the Xifeng section, the distributions of magnetic lineation are not clustered well around the maximum in the contour area and have few remarkably long 10° sectors in the rose diagram that forms a girdle around the SE direction. Based on our comparison to the moderate water current model in Figure 8, we consider that a moderate wind caused rolling of some elongate particles turning them perpendicular to the wind direction; therefore, the magnetic lineation varies notably in its orientation and is spread all over the stereonet projection. The $K_{min}$, however, is still shifted toward the NW defining the summer monsoon propagation from the SE. The Xifeng section is situated on a large flat surface which is far from the mountains that characterize the Baicaoyuan section and the Yellow River terrace of the Yichuan section. Thus the Xifeng site is more open to the winds than the Baicaoyuan and Yichuan sites. The summer monsoon, unrestricted by mountains and river terrace, could change direction more easily on an open plain. The distributions of $K_{max}$ in Yichuan are intermediate between Baicaoyuan and Xifeng and only one primary direction could be identified in the SE direction. This means that the wind strength in the Yichuan area was stronger than in the Baicaoyuan area and weaker than in the Xifeng area; we classify the wind strength in the Yichuan area as weak-moderate.

In order to independently verify our summer monsoon model, we examined the AMS results from two other sections in the Loess Plateau. One section is described in the west of the Loess Plateau (Liu et al., 2008a) and other is studied near Xi'an (Thistlewood and Sun, 1991). The AMS results from these papers are included to Figure 10. Although we cannot quantify the wind strength without their dataset, their primary directions look identical to our weak to moderate wind summer monsoon model. Their samples represent multiple loess and paleosol layers and result demonstrates that the vertical minimum axes Kmin are tilted towards the NW direction and maximum axes Kmax are oriented mostly to the SE direction. It confirms our summer monsoon model that explains the AMS orientation in the central and western parts of the Chinese Loess Plateau. It is a matter of the future study to verify if the AMS signal from the northern parts of the Plateau fits in our model. The winter monsoon wind in the North is much stronger than the summer monsoon wind and the magnetic particle could be probably oriented during the winter only. Such scenario would result in the AMS ellipsoid orientations toward NW.

## 5. Conclusion

We have studied the AMS in three sections representing the most recent 130 kyr interval along a W–E transect in the Chinese Loess Plateau. The orientations of major and minor AMS axes of sedimentary particles in the studied loess and paleosol sequences were determined to evaluate the paleowind direction. AMS measurements were used to identify the paleowind direction in three eolian deposits in the Chinese Loess Plateau. In our model, the AMS ellipsoid orientation is determined by the moist summer monsoon rather than the dry winter monsoon as previously hypothesized. We consider that the stronger summer monsoon that brings almost all annual rainfall plays a major role in the orientation of near surface dust particles and in their final consolidation. Based on our model, the major stream of the paleowind over the last 130 kyr has been generally similar to the present day summer monsoon routes.

## Acknowledgments

The paper benefitted considerably from comments and suggestions of S. Spassov and two anonymous reviewers. We thank J. Sun, Y. Xu, X. Zhao, H. Qin, L.P. Koukhar and L. Tober for their help in the field and during laboratory measurements and M. Craig for her help in the text editing. The study was supported by NSERC and the China Institute of the University of Alberta (grants of V.K.) and the Chinese Academy of Sciences (grant of R. Zhu). The first version of the manuscript benefited greatly from discussions with M.E. Evans, Q. Liu and C. Deng.

## Appendix A. Suppelementary data

Supplementary data to this article can be found online at doi:10.1016/j.epsl.2010.09.026.

## References

An, Z., 2000. The history and variability of the East Asian paleomonsoon climate. Quatern. Sci. Rev. 19, 171–187.
An, Z., Kutzbach, J.E., Prell, W.L., Porter, S.C., 2001. Evolution of Asian monsoons and phased uplift of the Himalaya–Tibetan plateau since Late Miocene times. Nature 411, 62–66.
Balsley, J.R., Buddington, A.F., 1960. Magnetic susceptibility anisotropy and fabric of some Adirondack granites and orthogneisses. Am. J. Sci. 258A, 6–20.
Banerjee, S.K., Hunt, C.P., Liu, X.M., 1993. Separation of local signals from the regional paleomonsoon record of the Chinese loess plateau: a rock magnetic approach. Geophys. Res. Lett. 20, 843–846.
Bassinot, F.C., Labeyrie, L.D., Vincent, E., Quidelleur, X., Shackelton, N.J., Lancelot, Y., 1994. The astronomical theory of climate and the age of the Brunhes–Matuyama magnetic reversal. Earth Planet. Sci. Lett. 126, 91–108.
Constable, C., Tauxe, L., 1990. The bootstrap for magnetic susceptibility tensors. J. Geophys. Res. 95, 8383–8395.
Deng, C.L., 2008. Paleomagnetic and mineral magnetic investigation of the Baicaoyuan loess–paleosol sequence of the western Chinese Loess Plateau over the last glacial–interglacial cycle and its geological implications. Geochemistry Geophysics Geosystems 9, Q04034. doi:10.1029/2007GC001928.
Deng, C., Zhu, R., Verosub, K.L., Singer, M.J., Vidic, N.J., 2004. Mineral magnetic properties of loess/paleosol couplets of the central loess plateau of China over the last 1.2 Myr. J. Geophys. Res. 109, B01103. doi:10.1029/2003JB002532.
Evans, M.E., Heller, F., 2003. Environmental Magnetism: Principles and Applications of Enviromagnetics. Elsevier Science, Academic Press.
Graham, J.W., 1954. Magnetic anisotropy, an unexploited petrofabric element. Geol. Soc. Am. Bull. 65, 1257–1258.
Grannar, L., 1958. Magnetic measurements on Swedish varved sediments. *Arkiv, F, Geofysik* 3, 1–40.
Heller, F., Beat, M., Wang, J., Liu, H., Liu, T., 1987. Magnetization and Sedimentary History of Loess in the central Loess Plateau of China. In: Liu, T.S. (Ed.), Aspects of Loess Research. China Ocean Press, Beijing, pp. 147–163.
Hrouda, F., 1982. Magnetic anisotropy of rocks and its application in geology and geophysics. Surv. Geophys. 5, 37–82.
Hus, J.J., 2003. The magnetic fabric of some loess/palaeosol deposits. Phys. Chem. Earth 28, 689–699.
Jelinek, V., 1981. Characterization of the magnetic fabric of rocks. Tectonophysics 79, 63–67.
Lagroix, F., Banerjee, S.K., 2002. Paleowind directions from the magnetic fabric of loess profiles in central Alaska. Earth Planet. Sci. Lett. 195, 99–112.
Lagroix, F., Banerjee, S.K., 2004a. Cryptic post-depositional reworking of aeolian sediments revealed by the anisotropy of magnetic susceptibility. Earth Planet. Sci. Lett. 224, 453–459.
Lagroix, F., Banerjee, S.K., 2004b. The regional and temporal significance of primary aeolian magnetic fabrics preserved in Alaskan loess. Earth Planet. Sci. Lett. 225, 379–395.
Lagroix, F., Borradaile, G.J., 2000. Magnetic fabric interpretation complicated by inclusions in mafic silicates. Tectonophysics 325 (3–4), 207–225.
Li, T., 2006. The process and mechanism of the rise of the Qinghai–Tibet Plateau. Tectonophysics 260, 45–53.
Liu, X.M., Xu, T., Liu, T., 1988. The Chinese loess in Xifeng, II. A study of anisotropy of magnetic susceptibility of loess from Xifeng. Geophys. J. Int. 92, 349–353.
Liu, P., Jin, C.S., Zhang, S., Han, J.M., Liu, T.S., 2008a. Magnetic fabric of early Quaternary loess–paleosols of Lingdan Profile in Gansu Province and the reconstruction of the paleowind direction. Chin. Sci. Bull. 53 (9), 1450–1452.
Liu, Q., Roberts, A.P., Rohling, E.J., Zhu, R., Sun, Y., 2008b. Post-depositional remanent magnetization lock-in and the location of the Matuyama–Brunhes geomagnetic reversal boundary in marine and Chinese loess sequences. Earth Planet. Sci. Lett. 275, 102–110.
Maher, B.A., Taylor, R.M., 1988. Nature formation of ultra-fine magnetite in soils. Nature 336, 368–370.
Nagata, T., 1961. Rock Magnetism, 2nd edition. Maruzen, Tokyo. 350 pp.
Porter, S.C., 2001. Chinese loess record of monsoon climate during the last glacial–interglacial cycle. Earth Sci. Rev. 54, 115–128.
Porter, S.C., An, Z., 1995. Correlation between climate events in the North Atlantic and China during the last glaciation. Nature 375, 305–308.
Rees, A.I., 1965. The use of anisotropy of magnetic susceptibility in the estimation of sedimentary fabric. Sedimentology 4, 257–271.
Rees, A.I., Wooddall, W.A., 1975. The magnetic fabric of some laboratory deposited sediments. Earth Planet. Sci. Lett. 25, 121–130.
Rieser, A.B., Bojar, A.V., Neubauer, F., Genser, J., Liu, Y.J., Ge, X.H., Friedl, G., 2009. Monitoring Cenozoic climate evolution of northern Tibet: stable isotope constraints from the western Qaidam Basin, China. Int. J. Earth Sci. 98, 1063–1075.

Robin, P.F., Jowett, E.C., 1986. Computerized density contouring and statistical evaluation of orientation data using counting circles and continuous weighting functions. Tectonophysics 121, 207–223.
Stacey, F.D., 1960. Magnetic anisotropy of igneous rocks. J. Geophys. Res. 65, 2429–2442.
Tarling, D.H., Hrouda, F., 1993. The Magnetic Anisotropy of Rocks. CRC Press, Boca Raton, Fla. 217 pp.
Thistlewood, L., Sun, J., 1991. A paleomagnetic and mineral magnetic study of the loess sequence at Liujiapo, X'ian, China. J. Quat. Sci. 6, 13–26.
Wu, H.B., Chen, F.H., Wang, J.M., Cao, J.X., Zhang, Y.T., 1999. Study on the relationship between magnetic anisotropy of modern eolian sediments and wind direction. Chin. J. Geophys. 42 (1), 71–78.
Xie, Q., Chen, T., Xu, H., Chen, J., Ji, J., Lu, H., Wang, X., 2009. Quantification of the contribution of pedogenic magnetic minerals to magnetic susceptibility of loess and paleosols on Chinese Loess Plateau: Paleoclimatic implications. J. Geophys. Res. 114, B09101. doi:10.1029/2008JB005968.
Zhu, R., Liu, Q., Jackson, M.J., 2004. Paleoenvironmental significance of the magnetic fabrics in Chinese loess–paleosols since the last interglacial (<130 ka). Earth Planet. Sci. Lett. 221, 55–69.
Zhu, R., Liu, Q., Pan, Y., Deng, C., Zhang, R., Wang, X., 2006. No apparent lock-in depth of the Laschamp geomagnetic excursion: evidence from the Malan loess. Sci. China, Ser. D Earth Sci. 49, 960–967.
Zhu, R., Zhang, R., Deng, C., Pan, Y., Liu, Q., Sun, Y., 2007. Are Chinese loess deposits essentially continuous? Geophys. Res. Lett. 34, L17306. doi:10.1029/2007GL030591.